Supporting Information for

Formation of a Tetranickel Octacarbonyl Cluster from the CO_2 Reaction of a Zero-valent Nickel Monocarbonyl Species

Changho Yoo and Yunho Lee*

Center for Catalytic Hydrocarbon Functionalization. Institute of Basic Science (IBS), Daejeon 305-701, Republic of Korea.
Department of Chemistry, Korea Advanced Institute of Science and Technology, Daejeon 305-701, Republic of Korea.

Contents

Figure S1. ^{1}H NMR spectrum of $\{(PN^{COONa}P)Ni(CO)_2\}_4$ (**2**) in benzene-d_6 at room temperature.

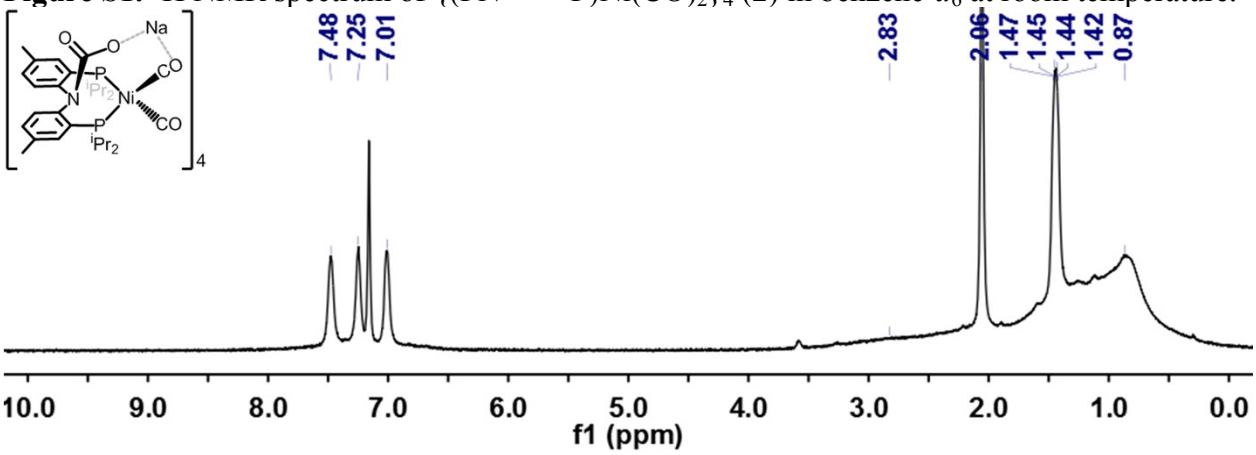

Figure S2. ^{13}C NMR spectrum of $\{(PN^{COONa}P)Ni(CO)_2\}_4$ (**2**) in benzene-d_6 at room temperature (●:pentane, ●:diethyl ether).

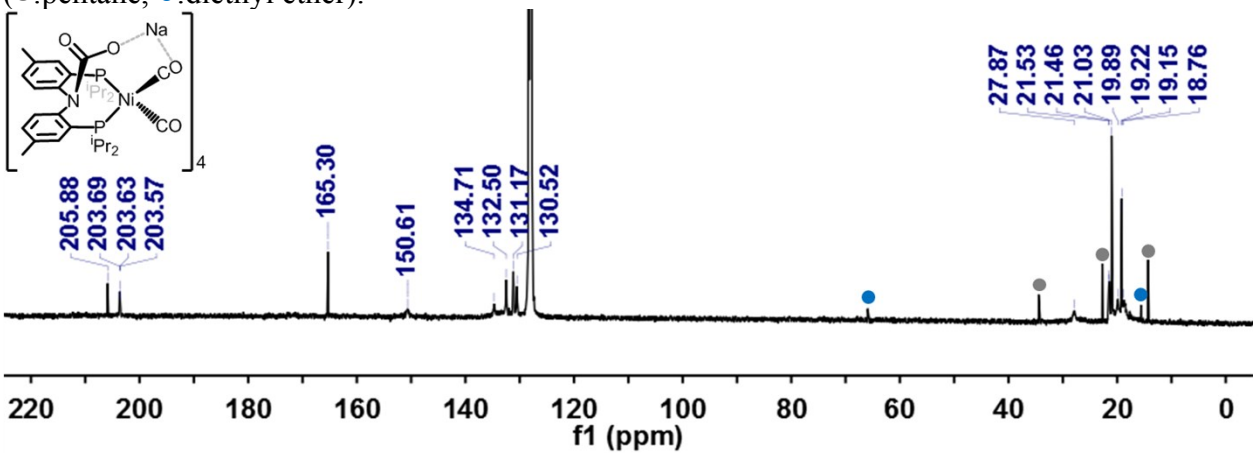

Figure S3. ^{31}P NMR spectrum of $\{(PN^{COONa}P)Ni(CO)_2\}_4$ (**2**) in benzene-d_6 at room temperature.

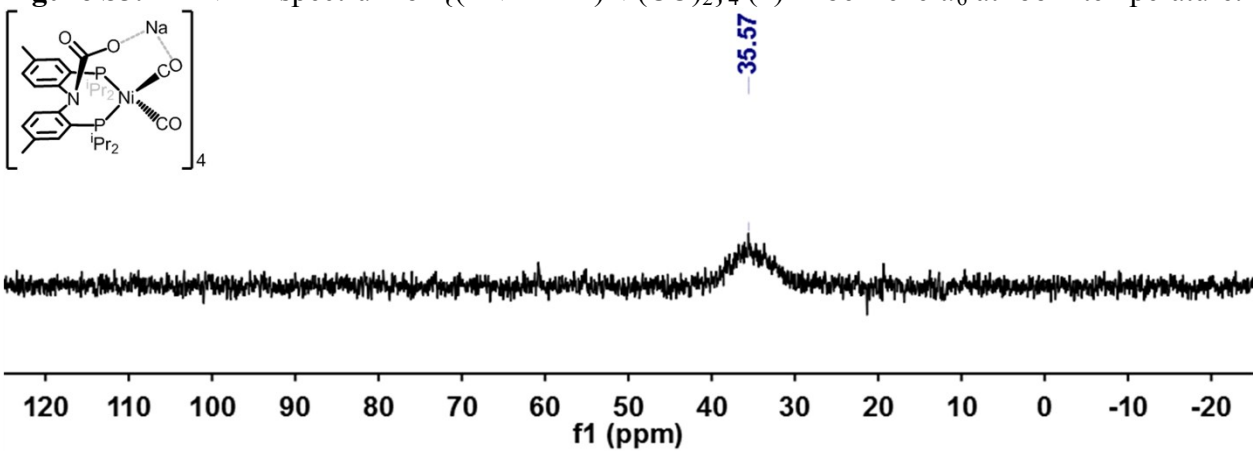

Figure S4. ^{1}H NMR spectrum of $\{(PN^{COONa}P)Ni(CO)_2\}_4$ (**2**) in THF-d_8 at room temperature (●:diethyl ether).

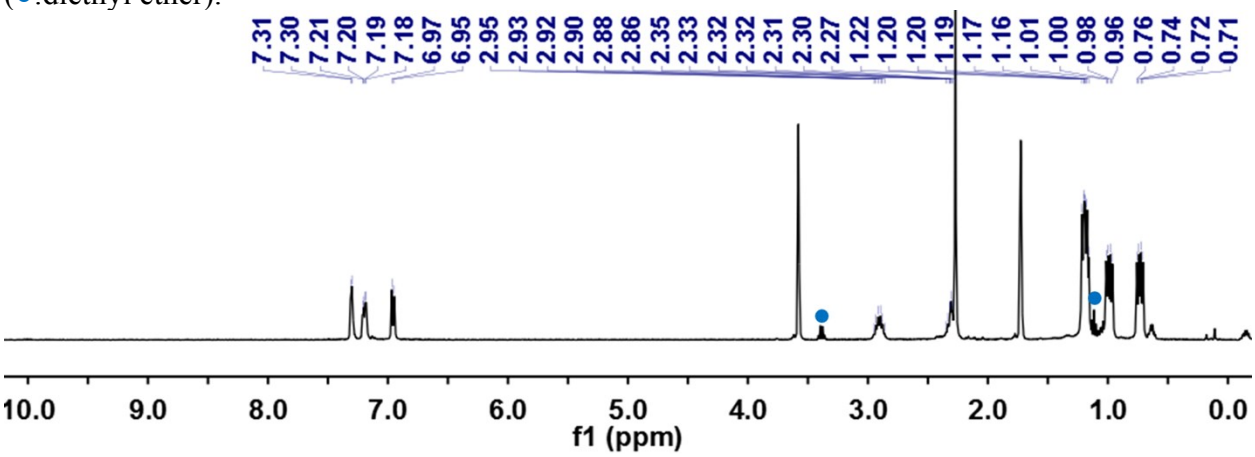

Figure S5. ^{13}C NMR spectrum of $\{(PN^{COONa}P)Ni(CO)_2\}_4$ (**2**) in THF-d_8 at room temperature.

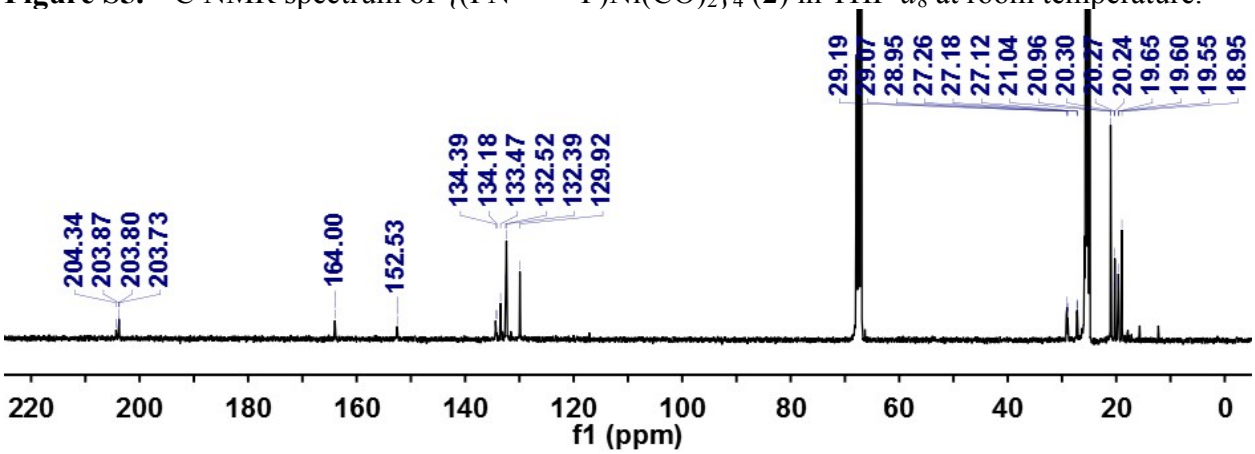

Figure S6. ^{31}P NMR spectrum of $\{(PN^{COONa}P)Ni(CO)_2\}_4$ (**2**) in THF-d_8 at room temperature.

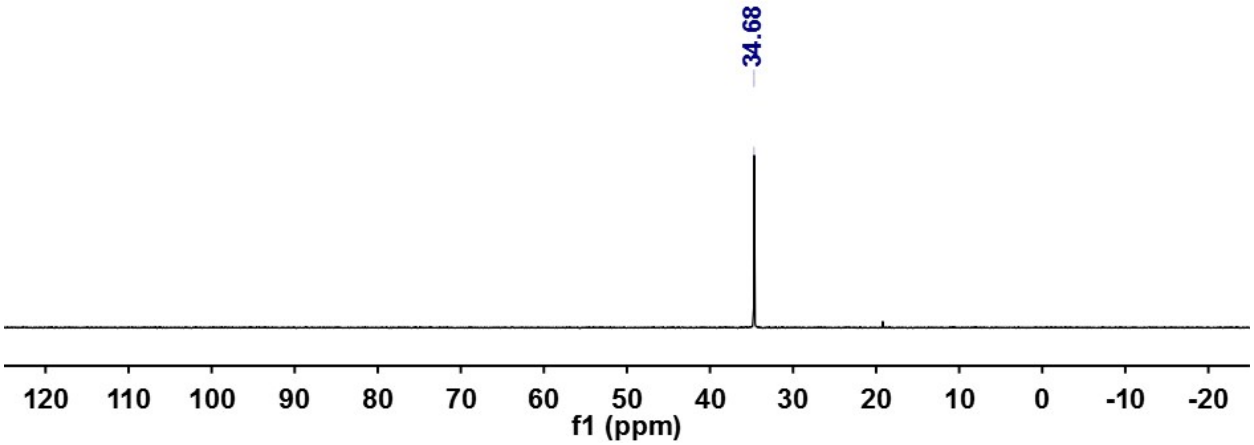

Figure S7. ^{1}H NMR spectrum of {(PNP)Ni}$_2$-μ-CO_3-κ^2*O,O* (**3**) in benzene-d_6 at room temperature (●:pentane).

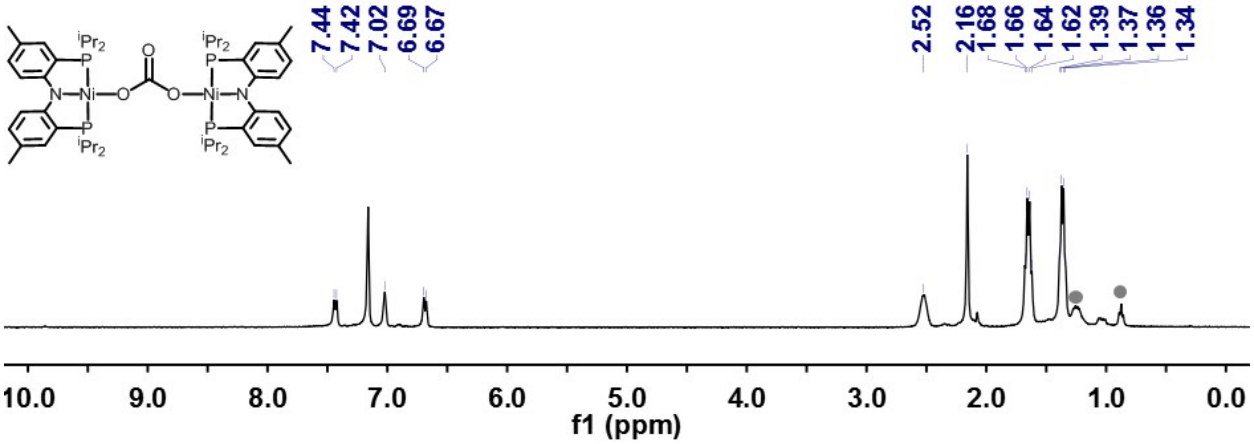

Figure S8. ^{13}C NMR spectrum of {(PNP)Ni}$_2$-μ-CO_3-κ^2*O,O* (**3**) in benzene-d_6 at room temperature (●:pentane).

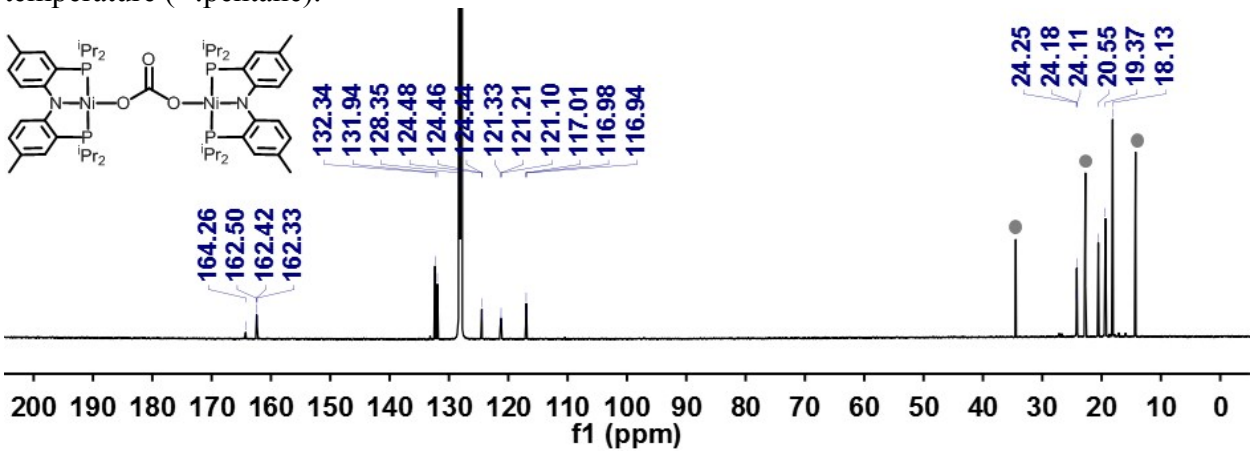

Figure S9. ^{31}P NMR spectrum of {(PNP)Ni}$_2$-μ-CO_3-κ^2*O,O* (**3**) in benzene-d_6 at room temperature.

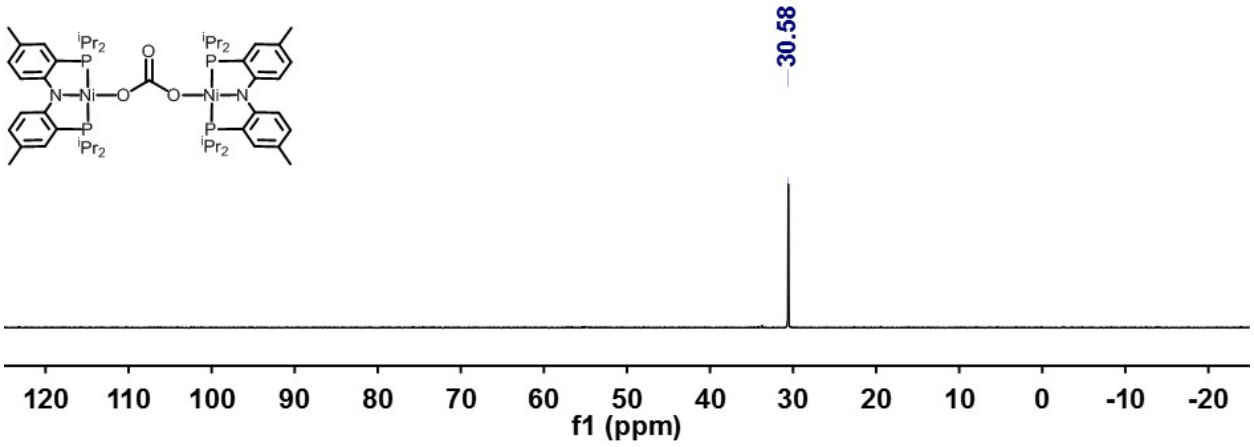

Figure S10. ^{13}C NMR spectrum (collected in THF/benzene-d_6, 162 MHz at room temperature) of the reaction of **1** with $^{13}CO_2$.

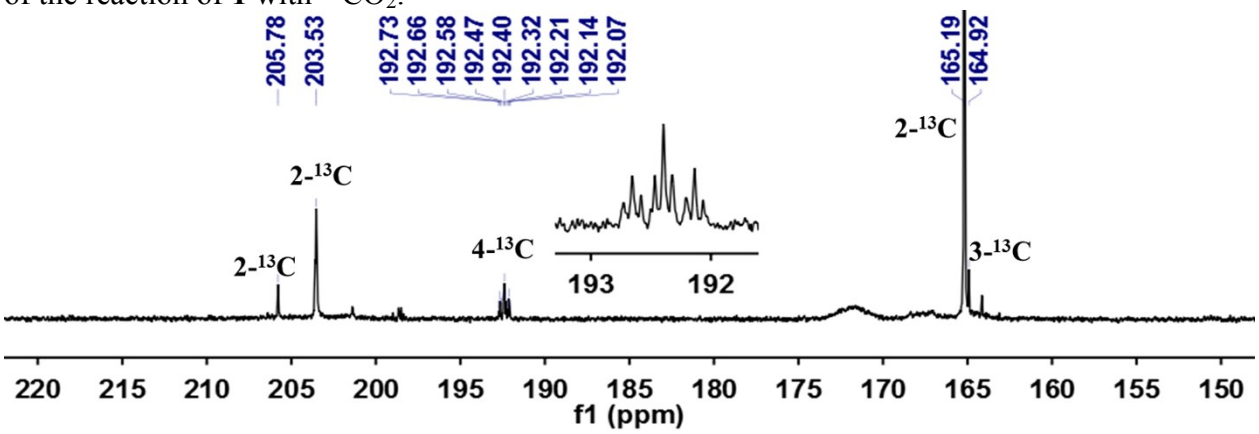

Figure S11. ^{13}C NMR spectrum of $\{(PN^{13COONa}P)Ni(CO)_x(^{13}CO)_{2-x}\}_4$ (**2-$^{13}CO_2$**) in benzene-d_6 at room temperature (●:pentane).

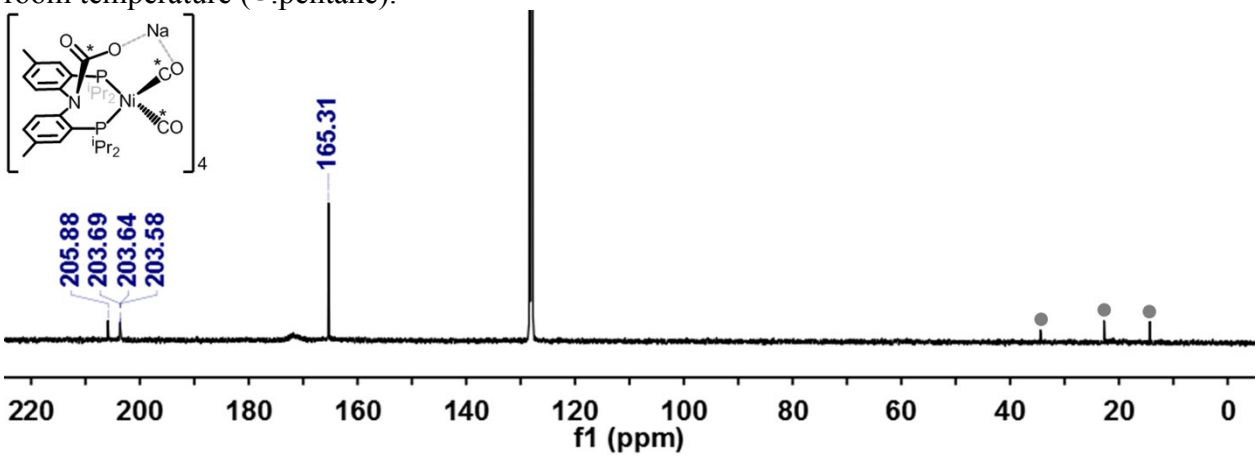

Figure S12. ^{13}C NMR spectrum of $\{(PN^{COONa}P)Ni(CO)_2\}_4$ (**2**, top) and $\{(PN^{13COONa}P)Ni(CO)_x(^{13}CO)_{2-x}\}_4$ (**2-$^{13}CO_2$**, bottom) in benzene-d_6 at room temperature. The relative intensities of both two carbonyl peaks at 203.64 and 205.88 ppm compared to a carbamate signal at 165.31 ppm decrease in **2-$^{13}CO_2$**, indicating both ^{12}CO and ^{13}CO are distributed over two different positions.

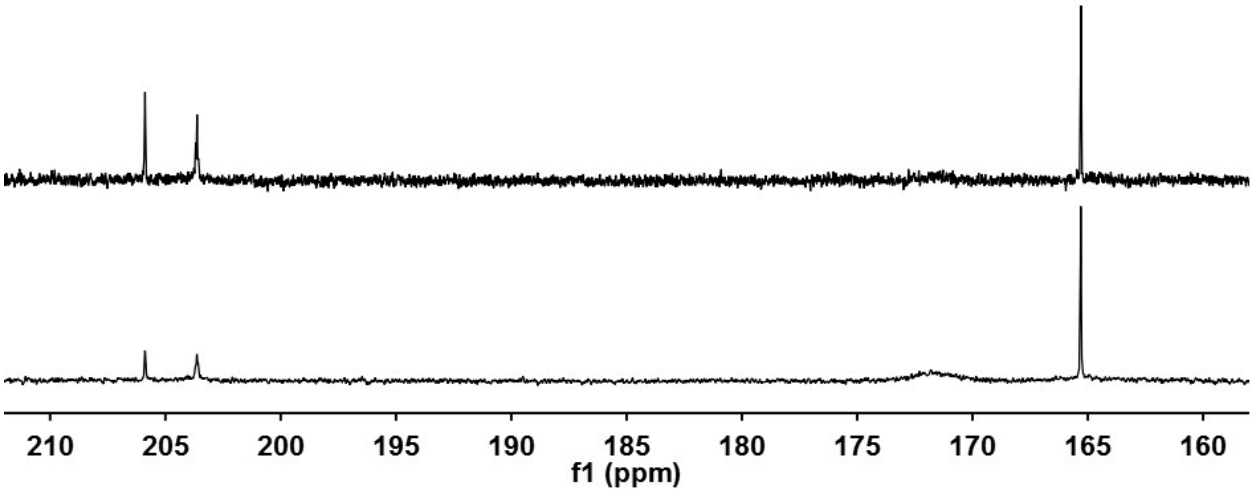

Figure S13. Single-pulse ^{31}P NMR spectrum (collected in THF/benzene-d_6, 162 MHz at room temperature) of the reaction of **1** (0.186 mmol) with CO_2. Triphenylphosphine oxide (0.093 mmol) was added as an internal integration standard. **2**: 0.022 mmol (48%); **3**: 0.0049 mmol (5.3%); **4**: 0.0077 mmol (8.3%); **6**: 0.0051 mmol (2.8%).

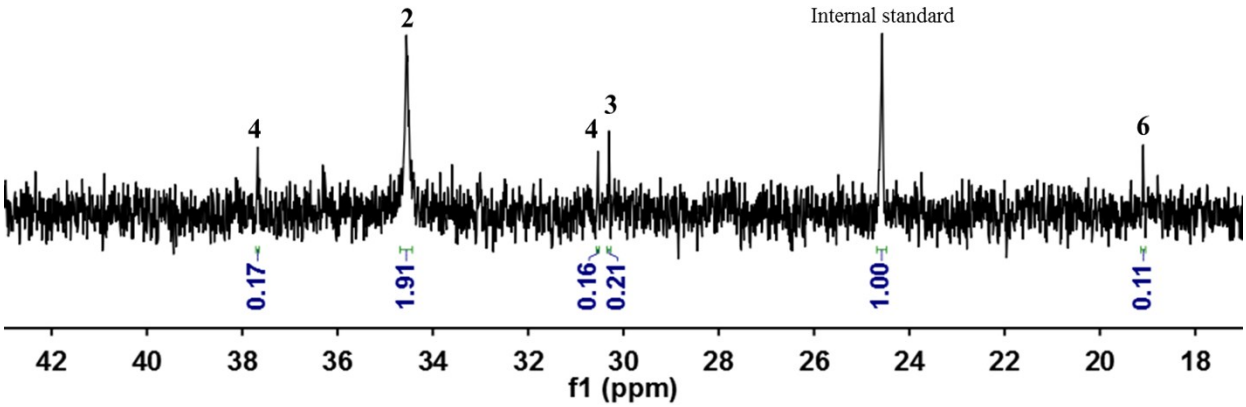

Figure S14. Plots of the normalized signal intensities (I/I_0) versus gradient strength (G) (top) and plots of $\ln(I/I_0)$ versus G^2 (bottom). The corresponding data obtained from pulsed gradient spin echo experiments for $\{(PN^{COONa}P)Ni(CO)_2\}_4$ (**2**, blue), $\{(PNP)Ni\}_2$-μ-CO_2-κ^2*C,O* (**4**, red) and $(PN^{H}P)Ni(CO)_2$ (**6**, green) in benzene-d_6 at room temperature.

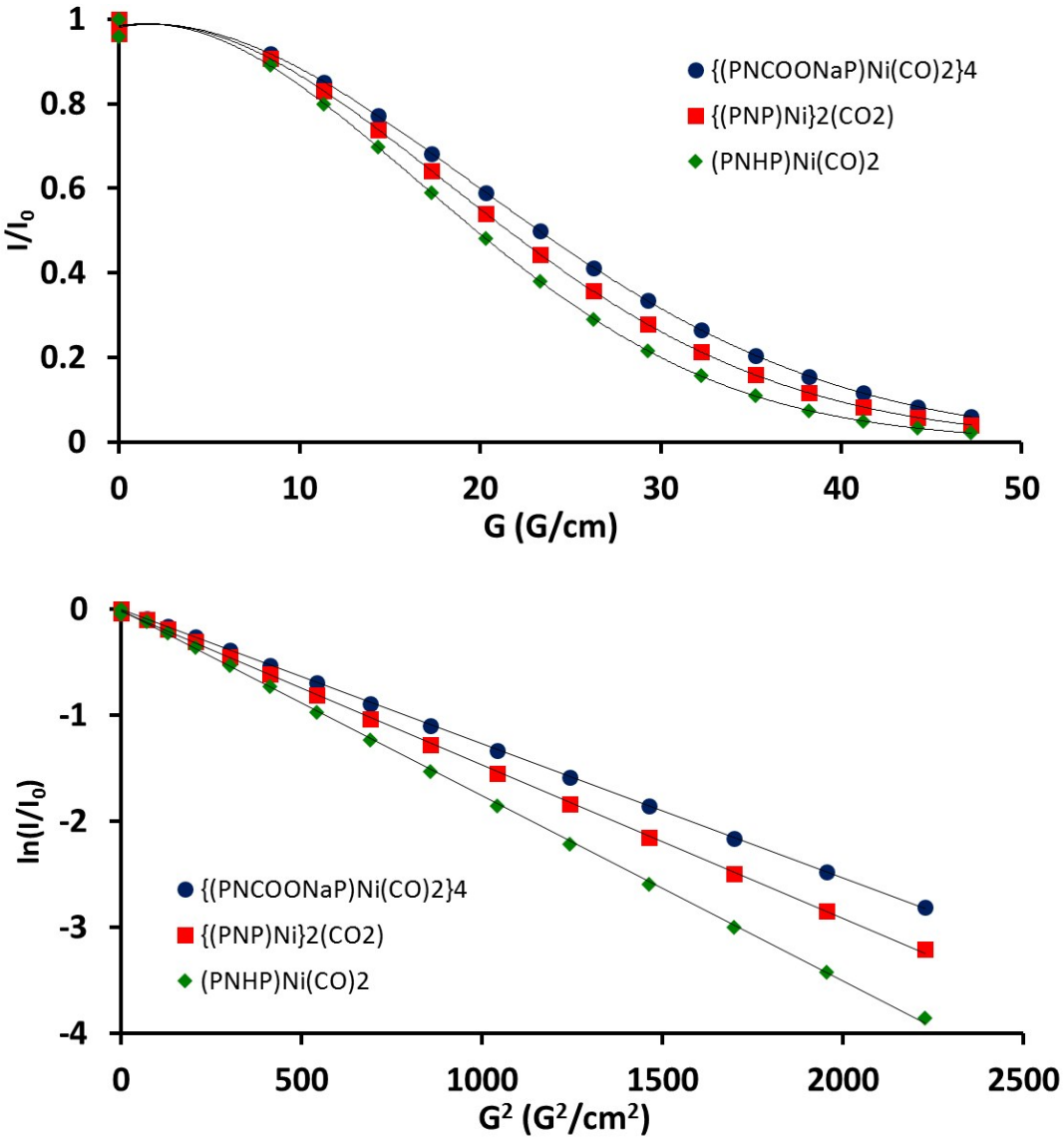

Table S1. Diffusion constants, hydrodynamic radii ($R_{solution}$) and solid state radii (R_{Solid}) for **2**, **4** and **6**.

Compound	Diffusion constant ($\times 10^{-10}$ m^2/s)	$R_{solution}$ (Å)	R_{Solid} (Å)[a]
2	4.877	7.366	8.8640
4	7.737	4.643	7.0172[b]
6	10.79	3.329	5.5155

[a] R_{Solid} is derived from the molecular volume; $R_{Solid} = (3V/4\pi)^{1/3}$. The molecular volume (V) is estimated by the following equation: V = the unit cell volume – the void volume calculated by PLATON.[1]

[b] This value is overestimated, since the crystal structure of **4** contains a co-crystallized ether molecule.

Figure S15. Solid state (R_{solid}, blue line) and solution state radii ($R_{solution}$, red line) for compound **2**, **4** and **6**.

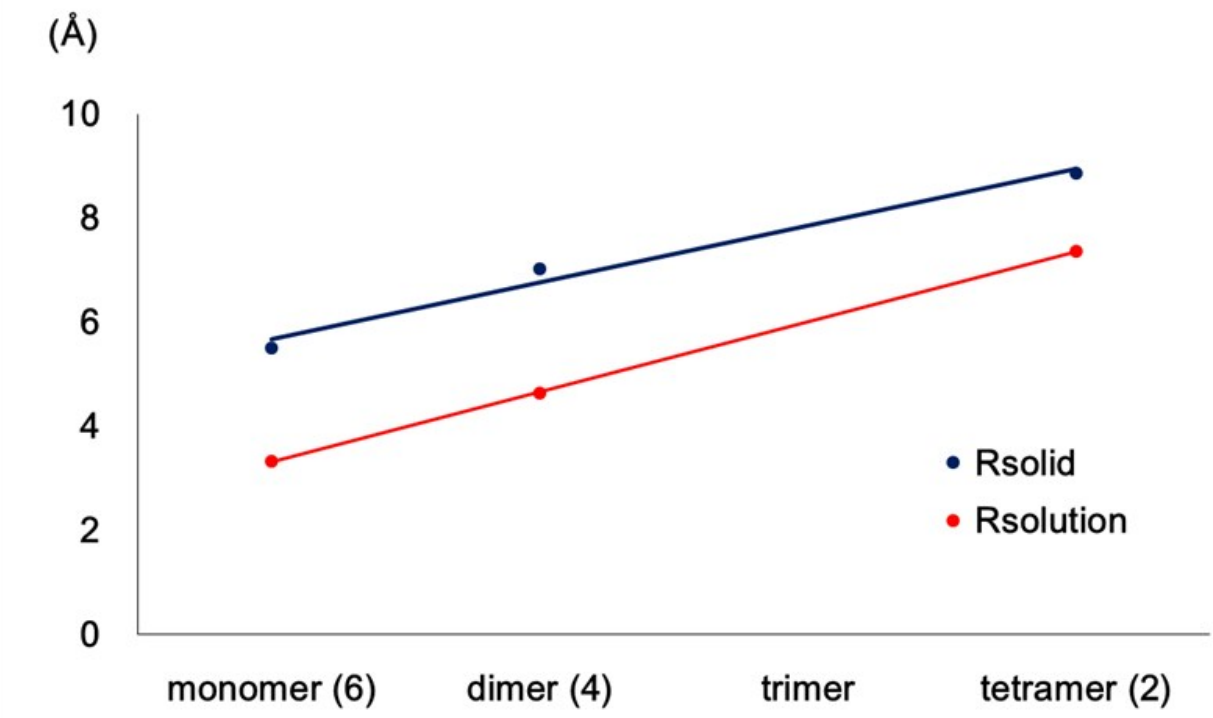

[1] (a) P. van der Sluis and A. L. Spek, *Acta Cryst.* 1990, **A45**, 194. (b) A. L. Spek, *PLATON, a Multipurpose Crystallographic Tool*, Utrecht University, The Netherlands, 2001.

Figure S16. IR spectra of $\{(PN^{COONa}P)Ni(CO)_2\}_4$ (**2**, blue line) and $\{(PN^{13COONa}P)Ni(CO)_x(^{13}CO)_{2-x}\}_4$ (**2-$^{13}CO_2$**, red line) (top) and the zoomed region of carbonyls and a carbamate vibration (bottom, KBr pellet).

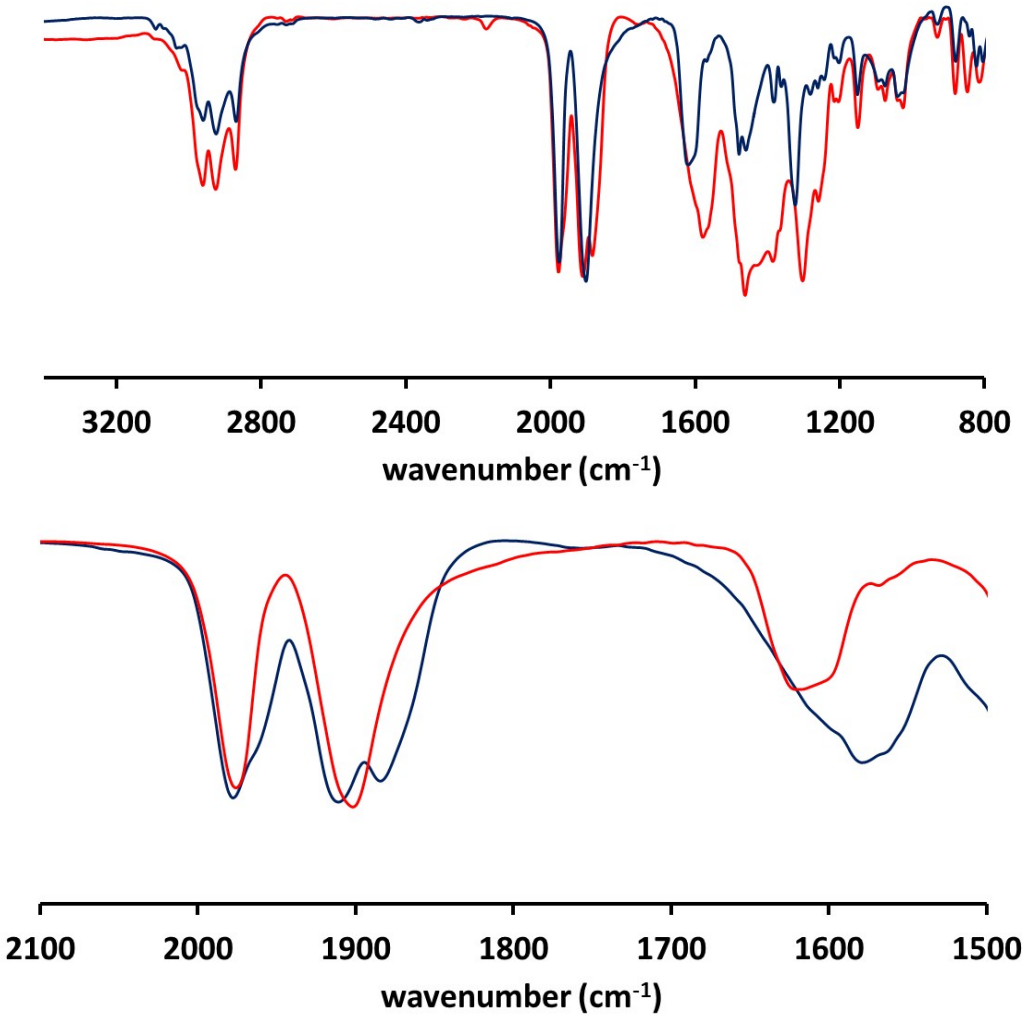

Figure S17. IR spectrum of $\{(PNP)Ni\}_2$-μ-CO_3-κ^2*O,O* (**3**) (KBr pellet).

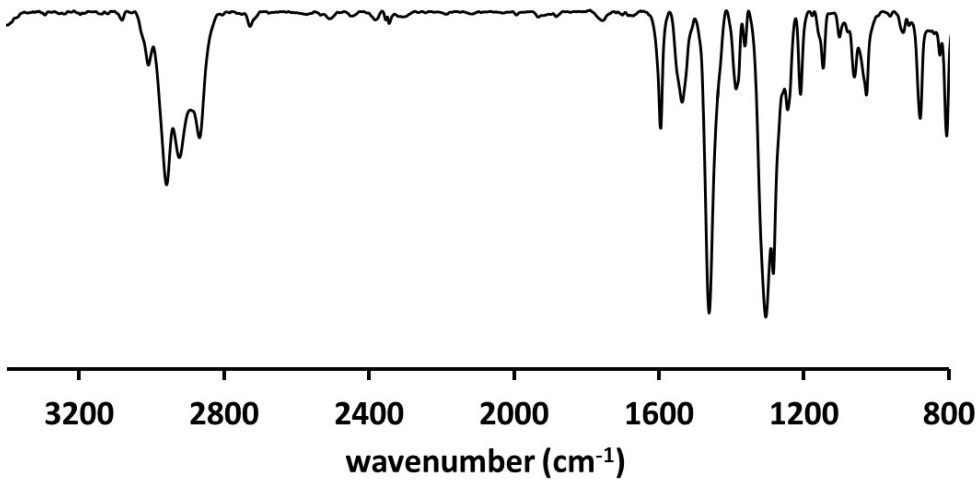

Figure S18. Solid-state structure of {Na}{(PNP)Ni(CO)} (**1**) in dimeric assembly with two co-crystallized THF molecules. Hydrogen atoms are omitted for clarity.

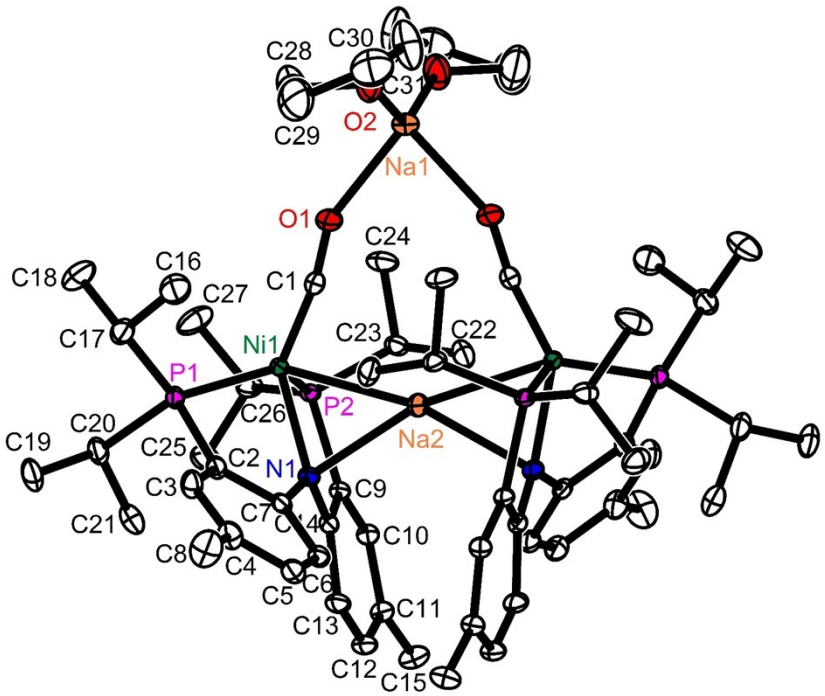

Table S2. Selected bond distances and angles for {Na}{(PNP)Ni(CO)} (**1**) with two co-crystallized THF molecules (Å and °).

Bond distance		Bond angle	
d_{Ni1-N1}	2.054(1)	∠N1-Ni1-C1	131.12(5)
d_{Ni1-C1}	1.711(1)	∠P1-Ni1-P2	127.48(2)
d_{Ni1-P1}	2.1883(4)	∠N1-Ni1-P1	83.36(3)
d_{Ni1-P2}	2.1799(5)	∠N1-Ni1-P2	86.21(3)
d_{C1-O1}	1.182(2)	∠C1-Ni1-P1	111.39(4)
d_{O1-Na1}	2.259(1)	∠C1-Ni1-P2	113.98(4)
d_{O2-Na1}	2.261(1)	∠Ni1-C1-O1	168.8(1)
$d_{Ni1-Na2}$	2.8523(5)		
d_{N1-Na2}	2.463(1)		

Figure S19. Solid-state structure of a monomer unit of **1** composed with {(PNP)NiCO}$^{-}$. Both sodium ions, Na1 with two co-crystallized THF molecules and Na2 interacting with nickel and nitrogen are shown; (a) side-, (b) top- and (c) front-view. Hydrogen atoms are omitted for clarity.

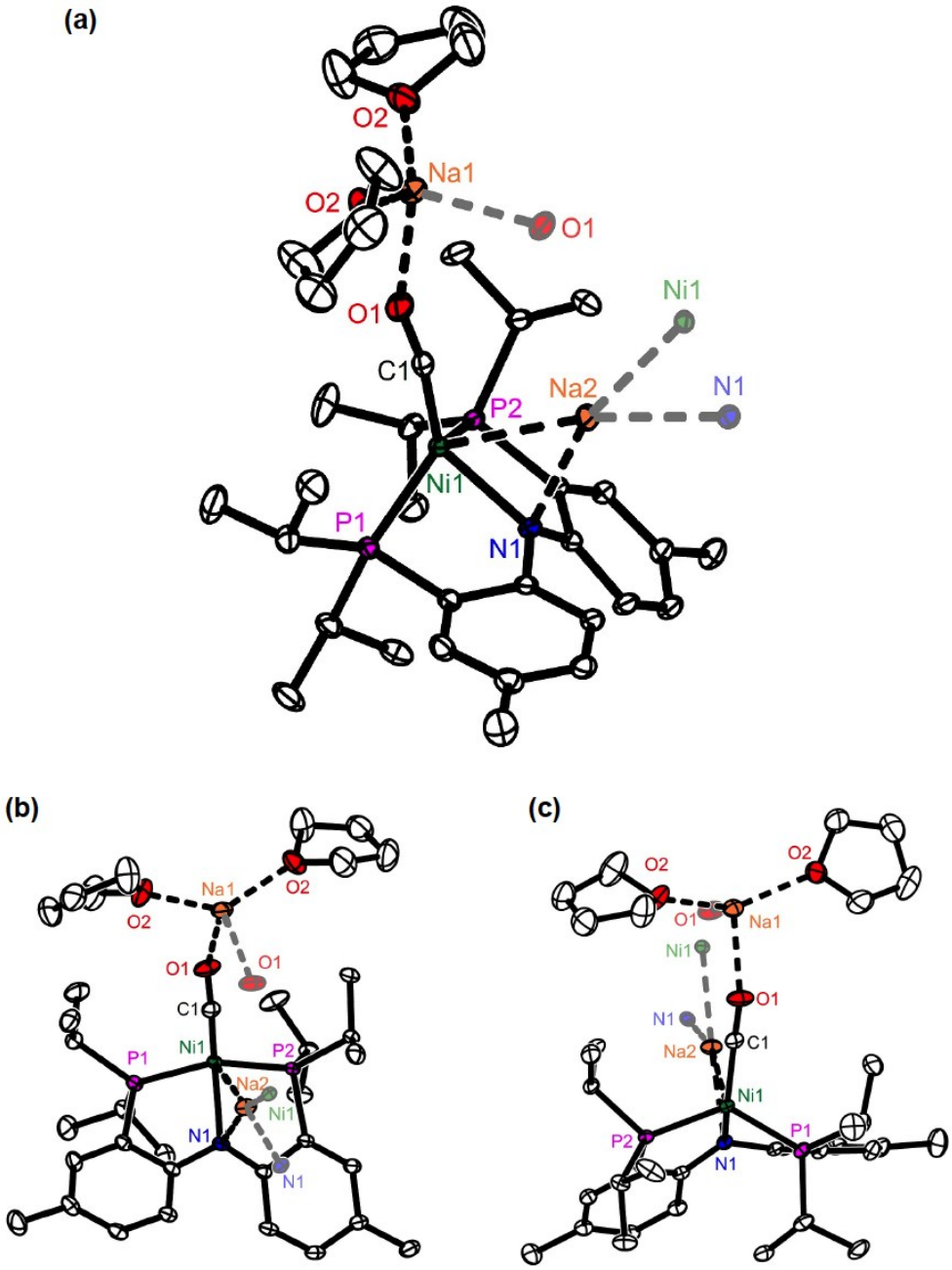

Figure S20. Solid-state structure of $\{(PN^{COONa}P)Ni(CO)_2\}_4$ (**2**). Hydrogen atoms are omitted for clarity.

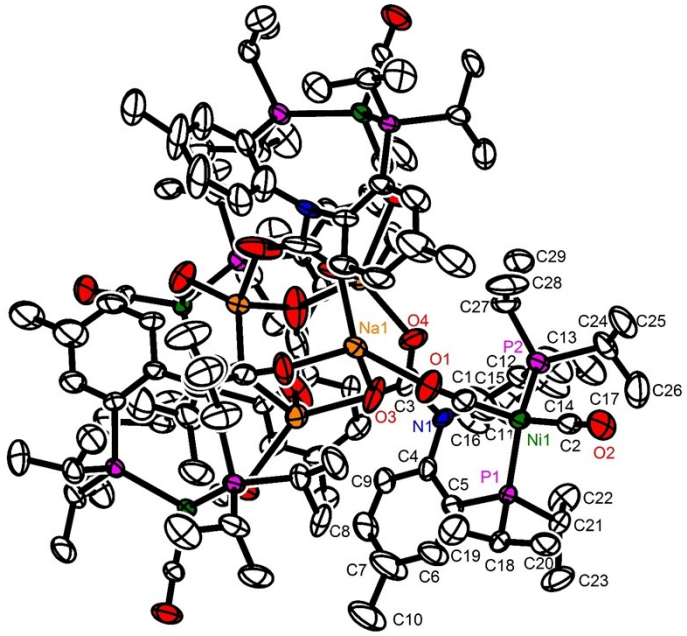

Table S3. Selected bond distances and angles for $\{(PN^{COONa}P)Ni(CO)_2\}_4$ (**2**) (Å and °).

Bond distance		Bond angle	
d_{Ni1-C1}	1.760(8)	∠C1-Ni1-C2	113.5(3)
d_{Ni1-C2}	1.752(7)	∠P1-Ni1-P2	112.78(7)
d_{Ni1-P1}	2.223(2)	∠C1-Ni1-P1	108.3(2)
d_{Ni1-P2}	2.218(2)	∠C1-Ni1-P2	106.1(2)
d_{Ni1-N1}	3.339(5)	∠C2-Ni1-P1	107.9(2)
d_{C1-O1}	1.132(8)	∠C2-Ni1-P2	108.4(2)
d_{C2-O2}	1.155(8)	∠Ni1-C1-O1	177.1(7)
d_{C3-O3}	1.25(1)	∠Ni1-C2-O2	178.0(7)
d_{C3-O4}	1.28(1)	∠O3-C3-O4	126.8(9)
d_{Na1-O1}	2.455(6)		
d_{Na1-O3}	2.243(6)		
d_{Na1-O4}	2.200(6)		

Figure S21. Solid-state structure of $\{(PNP)Ni\}_2$-μ-CO_3-κ^2*O,O* (**3**). Hydrogen atoms are omitted for clarity. The carbonate group was disordered over two distinct positions. For clarity, only one component is shown.

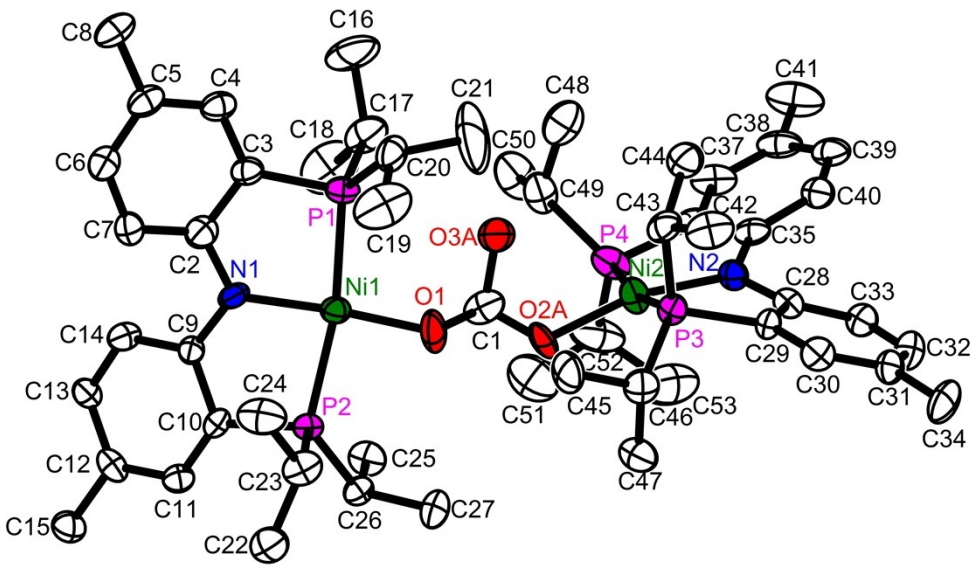

Table S4. Selected bond distances and angles for $\{(PNP)Ni\}_2$-μ-CO_3-κ^2*O,O* (**3**) (Å and °).

Bond distance		Bond angle	
d_{Ni1-O1}	1.828(7)	∠N1-Ni1-O1	175.6(4)
d_{Ni1-N1}	1.879(7)	∠P1-Ni1-P2	168.3(1)
d_{Ni1-P1}	2.206(2)	∠N1-Ni1-P1	85.6(2)
d_{Ni1-P2}	2.190(2)	∠N1-Ni1-P2	84.8(2)
$d_{Ni2-O3A}$	1.87(1)	∠N2-Ni1-O2A	164.2(5)
d_{Ni2-N2}	1.886(7)	∠P3-Ni1-P4	168.6(1)
d_{Ni2-P3}	2.179(2)	∠N2-Ni1-P3	85.7(2)
d_{Ni2-P4}	2.203(2)	∠N2-Ni1-P4	85.8(2)
d_{C1-O1}	1.24(1)	∠O1-C1-O2A	129(1)
d_{C1-O2A}	1.31(2)	∠O2A-C1-O3A	110(1)
d_{C1-O3A}	1.34(2)	∠O3A-C1-O1	115(1)

Figure S22. Solid-state structure of (PNP)Ni(CO) (**5**). Hydrogen atoms are omitted for clarity.

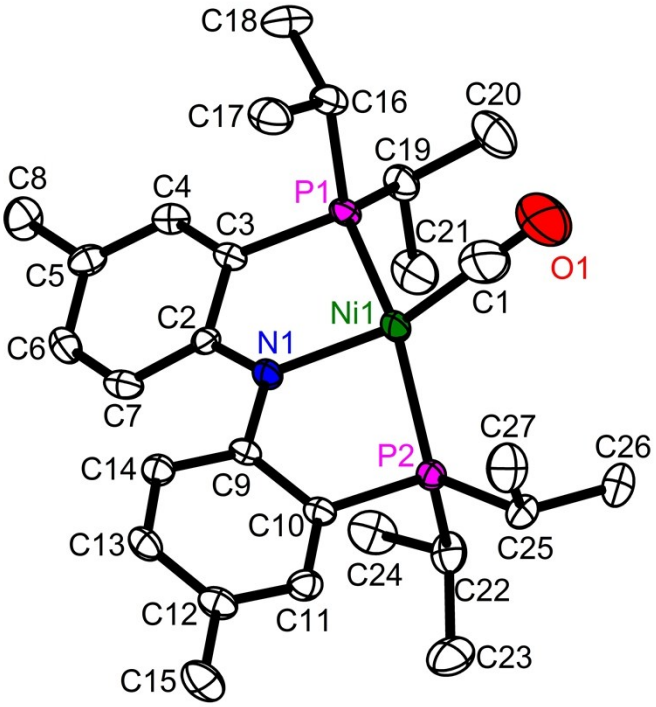

Table S5. Selected bond distances and angles for (PNP)Ni(CO) (**5**) (Å and °).

Bond distance		Bond angle	
d_{Ni1-N1}	1.962(3)	∠N1-Ni1-C1	149.3(3)
d_{Ni1-C1}	1.815(7)	∠P1-Ni1-P2	152.00(5)
d_{Ni1-P1}	2.215(1)	∠N1-Ni1-P1	85.5(1)
d_{Ni1-P2}	2.224(1)	∠N1-Ni1-P2	83.6(1)
d_{C1-O1}	1.119(7)	∠C1-Ni1-P1	98.7(2)
		∠C1-Ni1-P2	103.8(2)
		∠Ni1-C1-O1	171.3(7)

Figure S23. Solid-state structure of $\{(PNP)NiCOONa\}_2$•(THF). Hydrogen atoms are omitted for clarity.

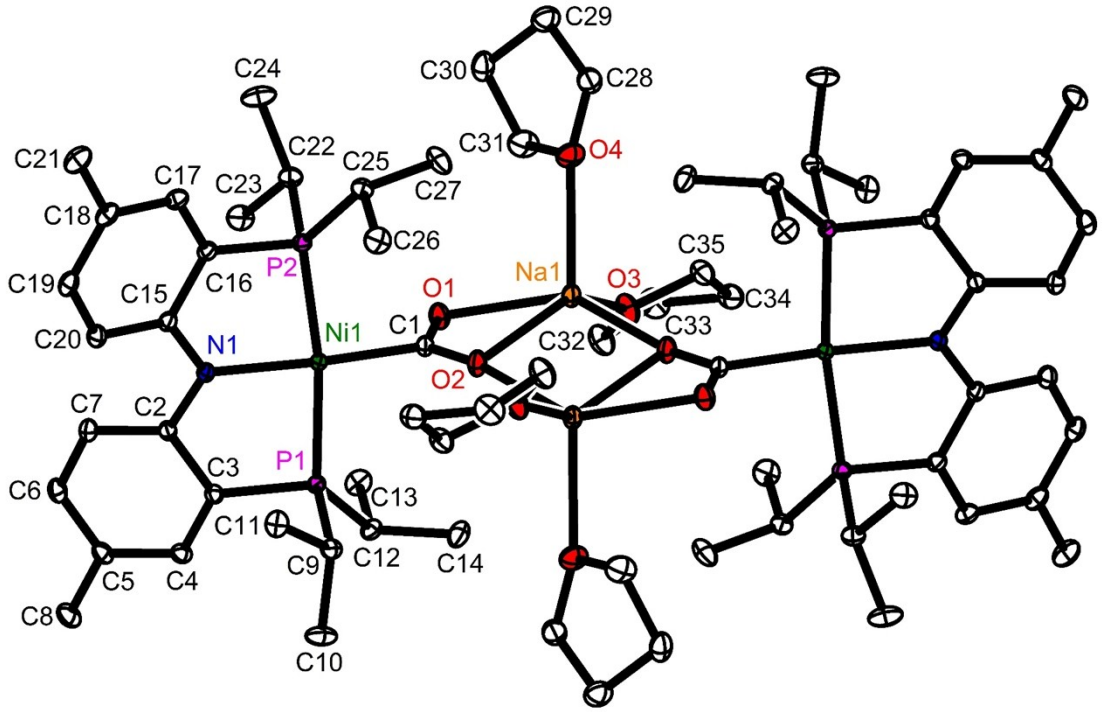

Table S6. Selected bond distances and angles for $\{(PNP)NiCOONa\}_2$•(THF) (Å and °).

Bond distance		Bond angle	
d_{Ni1-N1}	1.9611(9)	∠N1-Ni1-C1	174.30(5)
d_{Ni1-C1}	1.882(1)	∠P1-Ni1-P2	170.61(1)
d_{Ni1-P1}	2.1546(3)	∠N1-Ni1-P1	85.37(3)
d_{Ni1-P2}	2.1499(3)	∠N1-Ni1-P2	85.48(3)
d_{C1-O1}	1.260(1)	∠C1-Ni1-P1	96.46(3)
d_{C1-O2}	1.271(1)	∠C1-Ni1-P2	92.85(3)
d_{Na1-O1}	2.352(1)	∠O1-C1-O2	124.0(1)
d_{Na1-O2}	2.217(1)		
$d_{Na1-O2'}$	2.459(1)		
d_{Na1-O3}	2.290(1)		
d_{Na1-O4}	2.447(1)		